8. X. Zhang *et al.*, *Mol. Cell* **42**, 356–366 (2011).
9. J. Zhou *et al.*, *Mol. Gen. Genet.* **287**, 275–282 (2012).
10. D. Qutob, B. Patrick Chapman, M. Gijzen, *Nature Comm.* **4**, 1349 (2013).
11. N. Jiang, Y. Yang, G. Janbon, J. Pan, X. Zhu, *PLoS ONE* **7**, e52734 (2012).
12. H. C. Lee *et al.*, *Mol. Cell* **38**, 803–814 (2010).
13. C. C. Nunes *et al.*, *BMC Genomics* **12**, 288 (2011).
14. V. Raman *et al.*, *BMC Genomics* **14**, 326 (2013).
15. J. Amselem *et al.*, *PLOS Genet.* **7**, e1002230 (2011).
16. P. Veronese *et al.*, *Plant Cell* **18**, 257–273 (2006).
17. R. Schwab, S. Ossowski, M. Riester, N. Warthmann, D. Weigel, *Plant Cell* **18**, 1121–1133 (2006).
18. D. Ortiz-Masia, M. A. Perez-Amador, J. Carbonell, M. J. Marcote, *FEBS Lett.* **581**, 1834–1840 (2007).
19. Y. L. Liu, M. Schiff, S. P. Dinesh-Kumar, *Plant J.* **31**, 777–786 (2002).
20. S. J. Mi *et al.*, *Cell* **133**, 116–127 (2008).
21. T. A. Montgomery *et al.*, *Cell* **133**, 128–141 (2008).
22. J. B. Morel *et al.*, *Plant Cell* **14**, 629–639 (2002).
23. S. D. Kale *et al.*, *Cell* **142**, 284–295 (2010).
24. S. Wawra *et al.*, *Curr. Opin. Microbiol.* **15**, 685–691 (2012).
25. M. Rafiqi *et al.*, *Plant Cell* **22**, 2017–2032 (2010).
26. S. Schornack *et al.*, *Proc. Natl. Acad. Sci. U.S.A.* **107**, 17421–17426 (2010).
27. S. Wawra *et al.*, *Proc. Natl. Acad. Sci. U.S.A.* **109**, 2096–2101 (2012).
28. U. Ellendorff, E. F. Fradin, R. de Jonge, B. P. Thomma, *J. Exp. Bot.* **60**, 591–602 (2009).

Acknowledgments: We thank Y. Qi for AGO1 antibody; J. Carrington for the AGO1 and AGO2 tagged lines; H. Vaucheret for *ago1-27* mutant; M. J. Marcote for *mpk1 mpk2* seeds; and P. Karlovsky for pPK2 binary vector and *A. tumefaciens* strain AGL1 for *B. cinerea* transformation and gene knockout. This work was supported by an NIH grant (R01 GM093008), an NSF Career Award (MCB-0642843), an NSF award (IOS-1257576), and an AES-CE award (PPA-7517H) to H.J.; National Science Council of the Republic of China (NSC 101-2311-B-009-003-MY3 and NSC 100-2627-B-009-002) and UST-UCSD I-RiCE Program (NSC 101-2911-I-009-101) grants to H.-D.H.

Supplementary Materials

www.sciencemag.org/content/342/6154/118/suppl/DC1
Materials and Methods
Fig. S1 to S10
Tables S1 to S4
References (*29*–*32*)

26 April 2013; accepted 19 August 2013
10.1126/science.1239705

Crystal Structure of Na^+, K^+-ATPase in the Na^+-Bound State

Maria Nyblom,[1,2]*† Hanne Poulsen,[1,2,3]*‡ Pontus Gourdon,[1,2,3]* Linda Reinhard,[1,2]§ Magnus Andersson,[4] Erik Lindahl,[4,5] Natalya Fedosova,[1,6] Poul Nissen[1,2,3]‡

The Na^+, K^+–adenosine triphosphatase (ATPase) maintains the electrochemical gradients of Na^+ and K^+ across the plasma membrane—a prerequisite for electrical excitability and secondary transport. Hitherto, structural information has been limited to K^+-bound or ouabain-blocked forms. We present the crystal structure of a Na^+-bound Na^+, K^+-ATPase as determined at 4.3 Å resolution. Compared with the K^+-bound form, large conformational changes are observed in the α subunit whereas the β and γ subunit structures are maintained. The locations of the three Na^+ sites are indicated with the unique site III at the recently suggested IIIb, as further supported by electrophysiological studies on leak currents. Extracellular release of the third Na^+ from IIIb through IIIa, followed by exchange of Na^+ for K^+ at sites I and II, is suggested.

The Na^+, K^+–adenosine triphosphatase (ATPase) is typically a ternary complex of a large catalytic α subunit associated with two smaller subunits, β and γ (Fig. 1A). Different isoforms combine to form kinetically distinct complexes in different cells and tissues (*1*). During the ATP-driven transport cycle, three cytoplasmic Na^+ are exported in exchange for two extracellular K^+ through alternating E1/E1P and E2P/E2 states (Fig. 1B), where E1 and E2 denote high affinity for sodium and potassium ions, respectively, and P is phosphorylated. Intracellular Na^+ and ATP binding stimulate phosphorylation of a conserved aspartic acid residue (Asp^{369} in pig α_1 isoform; see alignment in fig. S1), forming the sodium-occluded $[Na_3]$E1P–adenosine diphosphate (ADP) state. Conformational changes and ADP release open an extracellular pathway in the E2P state, and Na^+ release and K^+ binding stimulate dephosphorylation, yielding the potassium-occluded $[K_2]$E2.P_i and $[K_2]$E2 states. Subsequent ATP binding and cytoplasmic K^+ release lead to the sodium-bound E1 states.

Previously, K^+-bound crystal structures representing the occluded E2.P_i state as mimicked by magnesium fluoride ($[K_2]$E2-MgF_x) (*2*, *3*) and structures with the inhibitory steroid ouabain (low-affinity $[K_2]$E2-MgF_x and high-affinity [Mg]E2P) have been elucidated (*4*, *5*). The intracellular C-terminal tail of the α subunit plays an important role in Na^+ binding (*2*, *6*–*10*), apparently by controlling an ion pathway (*6*, *7*), through a mechanism affected by many of the α_2 and α_3 isoform mutations that are associated with neurological diseases (*11*, *12*). However, further elucidation of the transport mechanism of the Na^+, K^+-ATPase has been limited by the lack of a structure of the Na^+-bound state, and in particular the location of the third Na^+ site has remained unsettled.

We present here the crystal structure determined at 4.3 Å resolution of the Na^+, K^+-ATPase in the $[Na_3]$E1P-ADP state (pig renal $\alpha_1\beta_1\gamma$ enzyme) as mimicked by an ADP-AlF_4^- complex (materials and methods and table S1) for which Na^+ saturation was further stabilized by the presence of oligomycin. The structure was determined from an unbiased electron density map derived by single isomorphous replacement with anomalous scattering (SIRAS), using hexatantalum dodecabromide (Ta_6Br_{12}) derivatized crystals, followed by density modification procedures (Fig. 1C and fig. S2). Model building using sharpened maps and restrained refinement produced a final model with R_{work} and R_{free} of 26.1 and 28.8%, respectively. The structure represents two nearly identical complexes in the asymmetric unit (chains A-B-G and C-D-E) and displays bilayer features in the electron density (figs. S2 to S4).

The ability of the E1-AlF_4^--ADP complex to occlude three Na^+ under crystallization-like conditions was confirmed by time-course measurements of $^{22}Na^+$ deocclusion at 0°C (Fig. 1F). The monoexponential fit resulted in the maximal number of 2.5 nmol of Na^+ per nmol of ADP binding sites (i.e., 83% occupancy) at 1 mM $^{22}Na^+$ and the deocclusion rate constant of 0.02 s^{-1}. Assuming a Hill coefficient of 3 for the cooperative Na^+ binding, the ion concentration required for the half-maximal saturation of the sites ($K_{0.5}$ for Na^+) was calculated to be 0.58 mM, consistent with previous findings (*13*). Thus, Na^+ concentration under crystallization conditions (>80 mM) was more than two orders of magnitude higher than the $K_{0.5}$, enough to saturate all three sites.

The α subunit represents a Na^+-occluded form of the transmembrane (TM) domain, with the cytoplasmic A, P, and N domains arranged for phosphorylation (Fig. 1, C and D) as observed for sarcoplasmic reticulum Ca^{2+} ATPase 1a (SERCA1a) in the equivalent, Ca^{2+}-occluded state (fig. S4B) (*14*–*16*). Thus, compared with K^+-bound forms, the α subunit is characterized by a different organization of the TM helices and a compact configuration of the cytoplasmic domains activating the phosphorylation site (Fig. 1, C and D, and fig. S5). Relative to the P domain, the A domain has undergone a rigid-body rota-

[1]Centre for Membrane Pumps in Cells and Disease–PUMPkin, Danish National Research Foundation, DK-8000 Aarhus, Denmark. [2]Department of Molecular Biology and Genetics, Aarhus University, Gustav Wieds Vej 10c, DK-8000 Aarhus, Denmark. [3]Danish Research Institute for Translational Neuroscience–DANDRITE, Nordic-EMBL Partnership of Molecular Medicine, Aarhus, Denmark. [4]Science for Life Laboratory, Theoretical and Computational Biophysics, Department of Theoretical Physics, Swedish e-Science Research Center, KTH Royal Institute of Technology, SE-171 21 Solna, Sweden. [5]Science for Life Laboratory, Department of Biochemistry and Biophysics, Stockholm University, SE-106 91 Stockholm, Sweden. [6]Department of Biomedicine, Aarhus University, Ole Worms Allé 4, Building 1182, DK-8000 Aarhus, Denmark.

*These authors contributed equally to this work.
†Present address: Novo Nordisk A/S, Novo Nordisk Park, B9.2.31, DK-2760 Maalov, Denmark.
‡Corresponding author. E-mail: hp@mb.au.dk (H.P.); pn@mb.au.dk (P.N.)
§Present address: Department of Cell and Molecular Biology, Karolinska Institutet, Box 285, SE-171 77 Stockholm, Sweden.

tion and translation, displacing by 45 Å the TGES (T, Thr; G, Gly; E, Glu; S, Ser) motif involved in dephosphorylation of Asp^{369}. Likewise, the N domain has rotated about 80° toward the P domain, stabilized by ADP-AlF_4^- at their interface (fig. S6). The P domain has rotated about 35° relative to the αM7 to αM10 (αM7-10) segment and moved together with the αM6-7 loop closer toward the TM region at the αC-terminal region (fig. S5).

The TM domain, which harbors the ion-binding sites and transport pathway, is formed by TM segments αM1-10, βM, and γM. Whereas αM7 to αM10 form a more rigid unit, αM1 αM6 are associated with significant structural rearrangements between K^+- and Na^+-bound conformations (Fig. 1 and fig. S7). The αM1-2 pair undergoes a rigid-body rotation toward αM9, the αM3-4 pair moves toward αM5-6 and translates toward the cytoplasmic side, whereas the cytoplasmic ends of αM5-6 move slightly toward the P domain with the extracellular portions nearly unchanged. This coupling of phosphorylation and occlusion of ion-binding sites at the TM domain, as communicated via tertiary interaction and connecting linkers, is the basis for the Na^+ specificity of the intramembranous ion-binding sites that characterizes the E1P state.

The β subunit has been proposed to undergo large conformational rearrangements relative to the α and γ subunits as part of the E2-to-E1 transition (*17*). However, in the [Na_3]E1-AlF_4^--ADP structure presented here, the β and γ subunits are not significantly changed compared to E2 states. The subunits are associated with the αM7-10 unit (figs. S1, S8, and S9), which is also seen to be fairly stable in SERCA1a (*18*, *19*). However, conformational changes of the quaternary structure may occur in the E1 intermediate state, which was recently described for the sarcolipin-bound complex of SERCA1a (*18*, *19*) (see below).

The Na^+, K^+-ATPase can bind three Na^+ at intramembranous binding sites (*20*), of which sites I and II have been localized to αM4-6 (*21*) by mutational studies and homology modeling based on the two Ca^{2+} sites of SERCA1a (*15*, *16*). In contrast, the binding position of the third Na^+ has remained enigmatic; two locations have been proposed on the basis of biochemical and electrophysiological studies: site IIIa between αM6, 8, and 9 and site IIIb between αM5, 7, and 8 (*6*, *7*, *22*–*24*) (Fig. 2A). Bound Na^+ cannot be directly observed at 4.3 Å resolution, but ion-binding sites often show characteristic features even at low resolution because of the coordinated assembly of side chains and ions that concentrate x-ray scatterers between transmembrane helices. This is evident for the expected Na^+ sites I and II, where we observe electron density compatible with occupancy at two sites between αM4 and αM6 (Fig. 2B and fig. S10). These sites are overall equivalent to the Ca^{2+} sites of SERCA1a (*15*), and the same residues also form the two K^+ sites in the [K_2]E2-P_i state (*4*, *11*) (Fig. 2, C and D).

The Na^+ site III is specific to the Na^+, K^+-ATPase, and we are not guided by SERCA1a homology. However, a notable electron density feature, reminiscent of that observed for sites I and II, is observed at the proposed site IIIb with residues Thr^{774}, Gln^{854}, Gln^{923}, and Asp^{926} between αM5, 7, and 8. In contrast, site IIIa, located adjacently with residues Glu^{954}, Tyr^{771} and Thr^{807},

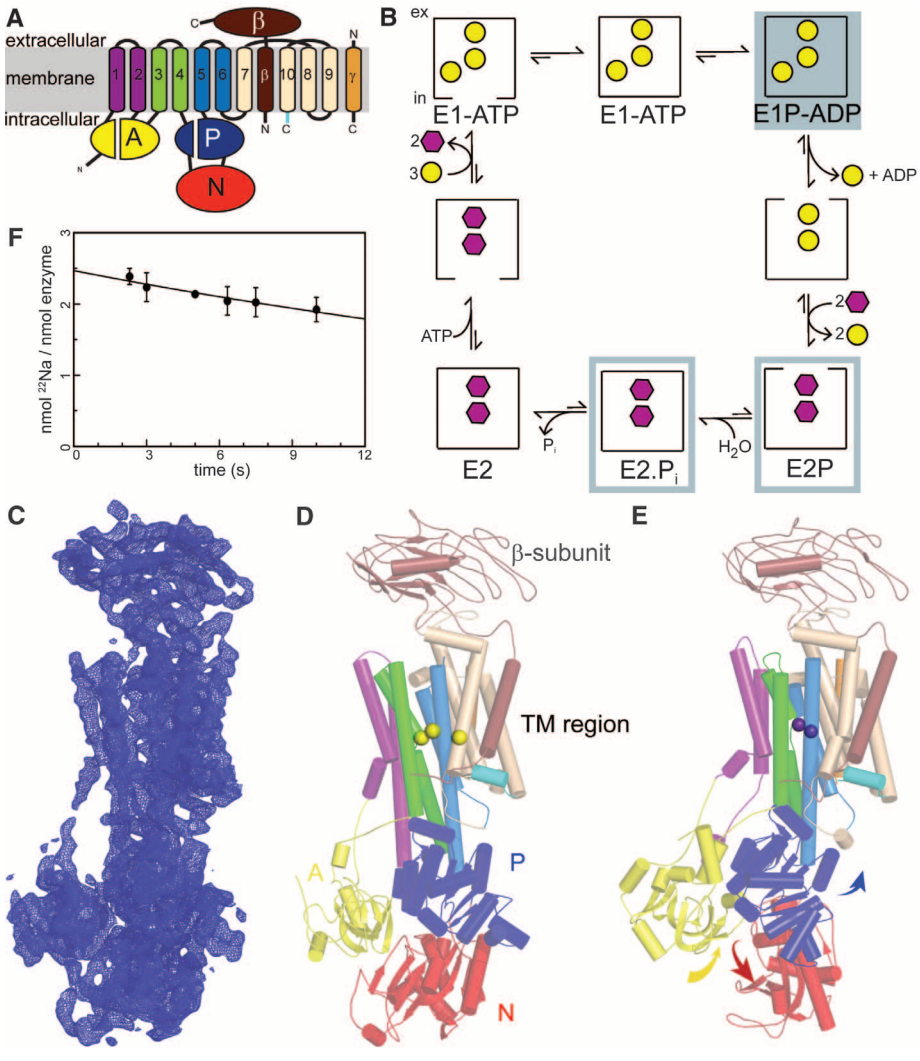

Fig. 1. Crystal structure of the Na^+, K^+-ATPase with bound sodium ions. (**A**) The α subunit is the major catalytic unit and contains three cytoplasmic domains: the A (actuator, yellow), N (nucleotide binding, red), and P (phosphorylation, blue) (*2*). The TM region encompassing 10 TM helices (αM1-10) harbors the ion-binding sites. The C-terminal helices αM7-10 are shown in wheat and the αC terminus in cyan. The mobile TM fragments, αM1-2, αM3-4, and αM5-6, are colored purple, green, and blue, respectively. The β subunit (in red-brown) has one TM helix (βM) and a highly glycosylated extracellular domain, and it is associated with αM7 and αM10. (**B**) Overview of the functional cycle of the Na^+, K^+-ATPase. Yellow circles and purple hexagons represent Na^+ and K^+ ions, respectively. E1P/E2P indicate the phosphoenzyme intermediates. Closed boxes represent occluded states, and ex and in are short for extracellular and intracellular, respectively. The gray boxes mark previously determined structures (*2*–*4*, *32*) (for E2P with ouabain), and the gray shaded box the state described here. (**C**) Final $2F_o - F_c$ electron density map of one αβγ complex (chains A, B, G) of the [Na_3]E1-AlF_4^--ADP crystal structure, displayed at 1.5σ contour level (blue mesh). (**D**) Cartoon representation in the same orientation as in (C) with the protein colored as in (A) and Na^+ as yellow spheres. (**E**) Cartoon representation of the [K_2]E2-MgF_x structure aligned with αM7-10 of the [Na_3]E1P-ADP state, colored as in (A), and with K^+ as purple spheres. The movements of the cytoplasmic domains relative to the [Na_3]E1P-ADP state are indicated by colored arrows. (**F**) Time dependence of $^{22}Na^+$ dissociation from the pig kidney enzyme preincubated with 1 mM $^{22}Na^+$ in the presence of oligomycin, ADP, and AlF_4^-. The molar ratio of 2.5 obtained by extrapolation of the curve to time 0 argues for full saturation of all three sites at crystallization conditions (>80 mM Na^+). Error bars indicate the standard deviation based on three independent experiments.

shows no indications of being coordinated as a Na^+-bound site (figs. S10 and S11). Thus, we infer that site IIIb corresponds to Na^+ site III (Fig. 2, B and C). In support, two independent 45-ns molecular dynamics (MD) simulations yield a stable structure with Na^+ bound at site IIIb (fig. S12).

Mutational studies were previously unable to distinguish unambiguously between IIIa and IIIb, because mutation at either site lowers the rate of extracellular sodium rebinding to a similar extent (*6*); sodium affinity, though, is lowered more for IIIb mutants (*6*, *7*, *22*–*24*). To shed light on the roles of sites IIIa and IIIb, we performed electrophysiological studies of a characteristic leak current, which is tightly coupled to both sites (*6*, *24*). The leak is an inwardly rectifying current, blocked by physiological levels of sodium or potassium and sensitive to the pump inhibitor ouabain (*25*). The leak is generally reduced by mutations in site IIIa (*24*), and it depends critically on Asp^{926} of IIIb; the Asp→Asn at position 926 (Asp926Asn) mutation blocks the leak at attainable voltages, presumably with the asparagine mimicking a constitutively protonated aspartate (*6*).

We examined the effects of mutations in either IIIa or IIIb more closely. Both of the IIIa mutants, Tyr771Phe and Glu954Ala, behaved similar to wild type: They leaked in the absence of extracellular sodium (albeit to a lesser extent), and the leak was closed by extracellular sodium (Fig. 3). In contrast, mutating Asp^{926} of IIIb to alanine gave no measurable leak in the absence of sodium but tiny leaks in the presence of sodium, whereas both Asp926Glu and Gln854Asn (IIIb) leaked with and without sodium.

Thus, although mutation of either site causes slower sodium rebinding and lower affinity (*6*), there is a discernible difference in the roles that the two sites play in leaking. IIIb mutants are less sensitive to extracellular sodium, whereas IIIa mutations cause less leakage overall (Fig. 3). This is consistent with the two sites acting in concert with Na^+ binding tightly at IIIb and IIIa being a transient site for extracellular sodium release and rebinding as well as for the leak current. A mutated IIIa would therefore have lower affinity, especially for extracellular sodium, but once bound Na^+ at site IIIb would be favorably coordinated and also block the leak of IIIa mutants (Fig. 3). Consistent with a transient role for site IIIa, it was recently shown that deletion of a helical turn including Glu^{954} maintained forward pumping (*26*), albeit at a reduced level, which suggests that a 3:2 ratio of sodium to potassium is most likely possible even with a highly compromised site IIIa.

Binding of the third Na^+ at IIIb is expected to block the leak, because it depends on Asp^{926} as a stepping stone, raising the question whether sodium can escape the mutated site and leak into the cytoplasm (Fig. 4A). Binding of the third Na^+ is strongly voltage dependent, so hyperpolarizing potentials favor occupancy at site IIIb, and, if Na^+ were not able to leak from a mutated site IIIb, increasingly hyperpolarizing potentials would be expected to eliminate leaking in the presence of sodium. However, the opposite is observed, which favors that a destabilized IIIb allows Na^+ to slip past the Asp^{926} checkpoint and enter the cytoplasm.

The exchange of Na^+ between the stable IIIb and a transient site IIIa would be dynamic and associated with conformational changes that allow extracellular release from IIIa. Additionally, Glu^{954} of IIIa is located at the αM2, 6, and 9 cleft, which binds sarcolipin in SERCA (*18*, *19*), and the neighboring Glu^{953} interacts directly with the γ subunit associated with αM9 (Fig. 4B). We find it likely that γ subunit and other proteins of the so-called FXYD family (where F is Phe; X, any amino acid, Y, Tyr; D, Asp) exert their regulatory function on Na^+, K^+-ATPase activity by interference with site IIIa function.

Several mutations affecting the C-terminal structure encompassing site IIIb of the α_2 and α_3 isoforms have been observed for the neurological diseases rapid-onset dystonia with parkinsonism (RDP) (*12*), hemiplegic migraines (*27*), and alternating hemiplegia of childhood (AHC) (*28*, *29*). Particularly in AHC, the ion-binding sites are hot spots. More than a third of the cases are linked to mutation of α_3 Asp^{801} (equivalent of pig α_1 Asp^{804}) between sites I and II to an asparagine (*28*, *29*), but there is also a case of the IIIb aspartate (the

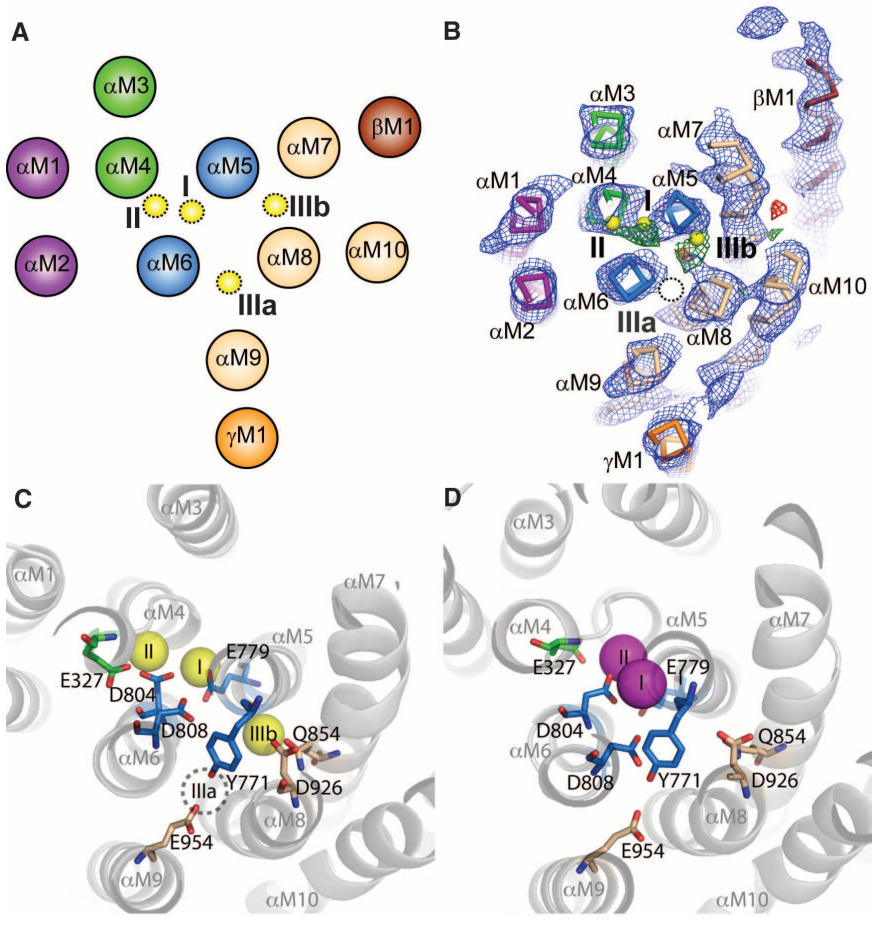

Fig. 2. The three Na^+ sites in the transmembrane domain. The protein is seen from the cytoplasmic side, about 90° rotated and colored as in Fig. 1. Key residues shown as sticks. (**A**) Schematic representation of the TM helices in the $[Na_3]$E1P-ADP state. The position and numbering of the proposed Na^+ sites (yellow spheres) are indicated. (**B**) For Na^+-binding sites I, II, and IIIb, unbiased electron density is visible between TM helices as seen from $F_o - F_c$ (contoured at ±4.5σ, green/red mesh) and $2F_o - F_c$ maps (contoured at 2.0σ, blue mesh; see figs. S10 to S12 for further information). (**C**) Ion-binding residues in the $[Na_3]$E1-AlF_4^--ADP form. Sodium ion positions are not accurate at the resolution of this study. TM helices are shown in white for clarity. Q, Gln. (**D**) Equivalent view as (C) for the $[K_2]$E2-MgF_x form (PDB code 3KDP).

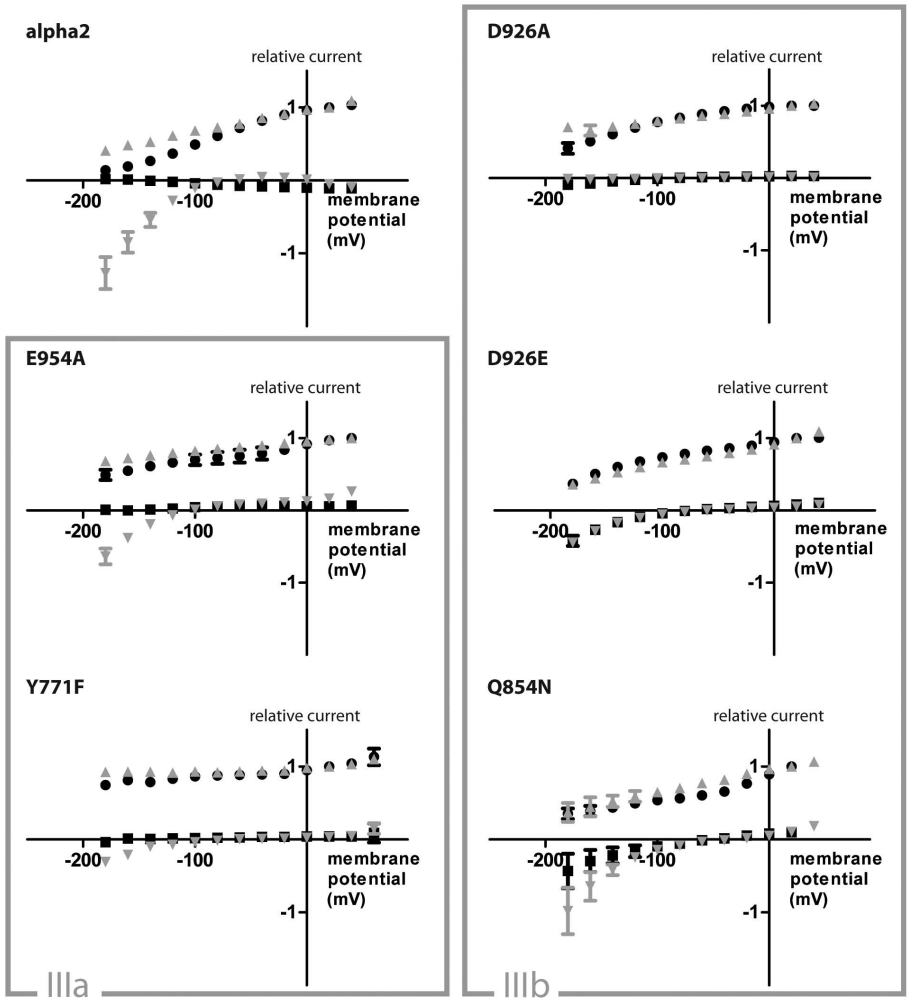

Fig. 3. Steady-state currents and leak currents of IIIa and IIIb mutants. Pump current is calculated as the ouabain-sensitive current in the presence of 15 mM potassium; the leak current is determined as the ouabain-sensitive current in the absence of potassium. Both pump and leak currents are normalized to the value of pump current at 20 mV. Pump currents in the presence (round black) and absence (gray up triangle) of 115 mM sodium as well as leak currents in the presence (square black) and absence (gray down triangle) of 115 mM sodium are shown. Error bars, SEM; $n = 3$ to 6 oocytes. Residue numbering corresponds to the pig α_1 isoform. Average of currents at 20 mV with/without sodium used for normalizations: E954A (A, Ala), 139 nAmp/101 nAmp; Y771F, 81 nAmp/109 nAmp; D926A, 92 nAmp/105 nAmp; D926E, 69 nAmp/61 nAmp; Q854N (N, Asn), 60 nAmp/61 nAmp.

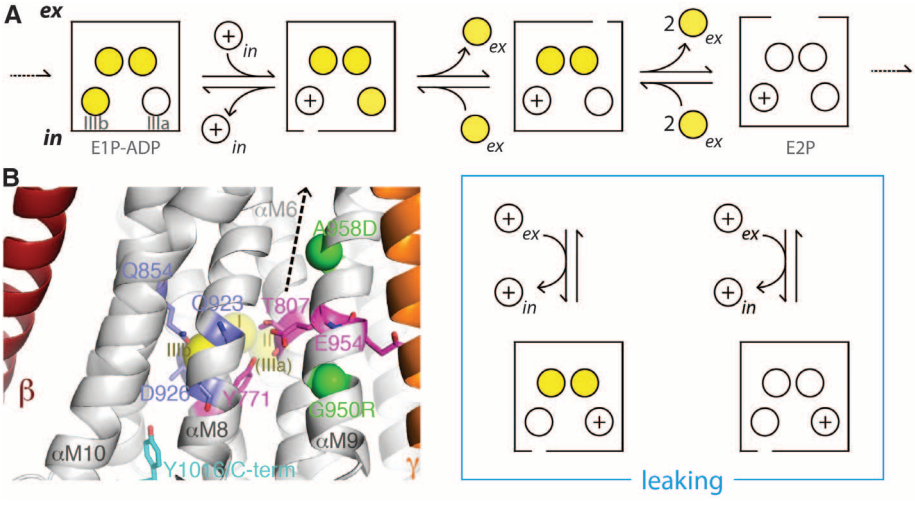

Fig. 4. Model for sodium release from Na^+, K^+-ATPase. (**A**) Schematic model illustrating extracellular sodium release and leaking. Na^+, yellow circle; proton, ⊕. The forward reaction is toward the right (full cycle in Fig. 1B). Extracellular release of Na^+ from IIIb is associated with protonation of Asp^{926} in a voltage-dependent reaction, so hyperpolarizing potentials promote the reverse reaction of Na^+ binding from the extracellular side to IIIb. The steps causing release of the other two sodium ions are less voltage sensitive (*20*). In the blue box, the proposed mechanism for proton leaking is indicated: An extracellular proton can bind site IIIa either in the presence of Na^+ at sites I and II (left) or in the absence of sodium (right), the IIIb proton is released intracellularly, and transfer of the IIIa proton to IIIb makes the site accessible for an extracellular proton again. Repeated extracellular binding and intracellular release of protons will create a leaking current. (**B**) Cartoon representation of the Na^+-binding sites (Na^+ in yellow spheres). Site IIIa and IIIb residues and the C terminus are indicated in magenta, blue, and cyan sticks, respectively, and the position of two AHC mutations by green spheres. A possible initial Na^+ release pathway through a transient site IIIa is indicated by a dashed arrow. Note the link between the γ subunit interface and site IIIa.

Asp^{926} here) mutated to a tyrosine (*29*). Mutation of the IIIb aspartate to asparagine was previously linked to RDP (*30*, *31*). Furthermore, two cases of AHC likely have perturbed IIIa function because the mutations are both one helical turn from Glu^{954} and cause a neutral residue to be substituted for a charged residue (Gly950Arg and Ala958Asp, pig α_1 residue numbers, Fig. 4B).

Proper binding and release of the third and electrogenic Na^+ of the Na^+, K^+-ATPase is essential for pump function, and the crystallographic and electrophysiological data presented here support a model in which Asp^{926} is the central ion-coordinating residue at site III as controlled by the C-terminal region and that Glu^{954} of a cooperative

site IIIa is associated with Na^+ release. High-resolution structures that accurately reveal Na^+ coordination and associated hydrogen-bonding networks will be essential for a better understanding of the structure-function relations of ion exchange, transport, and specificity and how the mechanism is affected by regulation and disease-related mutations.

References and Notes

1. G. Blanco, R. W. Mercer, *Am. J. Physiol.* **275**, F633–F650 (1998).
2. J. P. Morth *et al.*, *Nature* **450**, 1043–1049 (2007).
3. T. Shinoda, H. Ogawa, F. Cornelius, C. Toyoshima, *Nature* **459**, 446–450 (2009).
4. H. Ogawa, T. Shinoda, F. Cornelius, C. Toyoshima, *Proc. Natl. Acad. Sci. U.S.A.* **106**, 13742–13747 (2009).
5. M. Laursen, L. Yatime, P. Nissen, N. U. Fedosova, *Proc. Natl. Acad. Sci. U.S.A.* **110**, 10958–10963 (2013).
6. H. Poulsen *et al.*, *Nature* **467**, 99–102 (2010).
7. A. P. Einholm, M. S. Toustrup-Jensen, R. Holm, J. P. Andersen, B. Vilsen, *J. Biol. Chem.* **285**, 26245–26254 (2010).
8. S. Meier, N. N. Tavraz, K. L. Dürr, T. Friedrich, *J. Gen. Physiol.* **135**, 115–134 (2010).
9. N. Vedovato, D. C. Gadsby, *J. Gen. Physiol.* **136**, 63–82 (2010).
10. M. S. Toustrup-Jensen *et al.*, *J. Biol. Chem.* **284**, 18715–18725 (2009).
11. P. Blanco-Arias *et al.*, *Hum. Mol. Genet.* **18**, 2370–2377 (2009).
12. P. de Carvalho Aguiar *et al.*, *Neuron* **43**, 169–175 (2004).
13. M. Esmann, J. C. Skou, *Biochem. Biophys. Res. Commun.* **127**, 857–863 (1985).
14. C. Olesen *et al.*, *Nature* **450**, 1036–1042 (2007).
15. T. L. Sørensen, J. V. Møller, P. Nissen, *Science* **304**, 1672–1675 (2004).
16. C. Toyoshima, T. Mizutani, *Nature* **430**, 529–535 (2004).
17. R. E. Dempski, K. Hartung, T. Friedrich, E. Bamberg, *J. Biol. Chem.* **281**, 36338–36346 (2006).
18. A. M. Winther *et al.*, *Nature* **495**, 265–269 (2013).
19. C. Toyoshima *et al.*, *Nature* **495**, 260–264 (2013).
20. M. Holmgren *et al.*, *Nature* **403**, 898–901 (2000).
21. H. Ogawa, C. Toyoshima, *Proc. Natl. Acad. Sci. U.S.A.* **99**, 15977–15982 (2002).
22. T. Imagawa, T. Yamamoto, S. Kaya, K. Sakaguchi, K. Taniguchi, *J. Biol. Chem.* **280**, 18736–18744 (2005).
23. E. A. Jewell-Motz, J. B. Lingrel, *Biochemistry* **32**, 13523–13530 (1993).
24. C. Li, K. Geering, J. D. Horisberger, *J. Membr. Biol.* **213**, 1–9 (2006).
25. A. Vasilyev, K. Khater, R. F. Rakowski, *J. Membr. Biol.* **198**, 65–76 (2004).
26. E. A. Azizan *et al.*, *Nat. Genet.* **45**, 1055–1060 (2013).
27. M. De Fusco *et al.*, *Nat. Genet.* **33**, 192–196 (2003).
28. E. L. Heinzen *et al.*, *Nat. Genet.* **44**, 1030–1034 (2012).
29. H. Rosewich *et al.*, *Lancet Neurol.* **11**, 764–773 (2012).
30. I. A. Anselm, K. J. Sweadner, S. Gollamudi, L. J. Ozelius, B. T. Darras, *Neurology* **73**, 400–401 (2009).
31. P. Zanotti-Fregonara *et al.*, *J. Neurol. Sci.* **273**, 148–151 (2008).
32. L. Yatime *et al.*, *J. Struct. Biol.* **174**, 296–306 (2011).

Acknowledgments: B. Vilsen and J. Petersen, Department of Biomedicine, Aarhus University, Denmark, are thanked for preparing enzyme for crystallization. We thank C. Schulze-Briese, T. Tomizaki, and V. Olieric (Swiss Light Source) for assistance with synchrotron data collection; B. Bjerring Jensen, A. M. Nielsen, and J. L. Karlsen for technical assistance; and J. P. Morth, L. Yatime, M. Laursen, H. Khandelia, and M. J. Clausen for valuable discussions. Support was provided by the Danscatt program of the Danish Natural Science Research Council. M.N. was supported by the Swedish Research Council, L.R. by the Danish Council for Independent Research in Medical Sciences, E.L. by a European Research Council starting grant (contract 209825), and P.N. by a European Research Council advanced grant (contract 250322). H.P. was supported by the Lundbeck Foundation, the Carlsberg Foundation, and L'Oréal/United Nations Educational, Scientific, and Cultural Organization. The authors made the following contributions: H.P. and P.N. performed study design. M.N. crystallized the protein, collected and processed x-ray data, and determined and refined the structure, assisted by L.R. and P.G. The structural analysis was carried out by M.N., L.R., and P.G., assisted by P.N., whereas M.A. and E.L. performed the MD simulations, assisted by P.G. H.P. designed and performed the electrophysiological studies. N.F. designed and performed the deocclusion experiments. M.N., L.R., P.G., H.P., and P.N. wrote the paper. All authors discussed the results and commented on the manuscript. Coordinates and structure factors have been deposited in the Protein Data Bank (PDB) with accession no. 4hqj.

Supplementary Materials

www.sciencemag.org/content/342/6154/123/suppl/DC1
Materials and Methods
Figs. S1 to S12
Table S1
References (*33*–*58*)

17 July 2013; accepted 3 September 2013
10.1126/science.1243352

Quantifying Long-Term Scientific Impact

Dashun Wang,[1,2]* Chaoming Song,[1,3]* Albert-László Barabási[1,4,5,6]†

The lack of predictability of citation-based measures frequently used to gauge impact, from impact factors to short-term citations, raises a fundamental question: Is there long-term predictability in citation patterns? Here, we derive a mechanistic model for the citation dynamics of individual papers, allowing us to collapse the citation histories of papers from different journals and disciplines into a single curve, indicating that all papers tend to follow the same universal temporal pattern. The observed patterns not only help us uncover basic mechanisms that govern scientific impact but also offer reliable measures of influence that may have potential policy implications.

Of the many tangible measures of scientific impact, one stands out in its frequency of use: citations (*1*–*10*). The reliance on citation-based measures, from the Hirsch index (*4*) to the g-index (*11*), from impact factors (*1*) to eigenfactors (*12*), and on diverse ranking-based metrics (*13*) lies in the (often debated) perception that citations offer a quantitative proxy of a discovery's importance or a scientist's standing in the research community. Often lost in this debate is the fact that our ability to foresee lasting impact on the basis of citation patterns has well-known limitations.

1) The impact factor (IF) (*1*), conferring a journal's historical impact to a paper, is a poor predictor of a particular paper's future citations (*14*, *15*): Papers published in the same journal a decade later acquire widely different number of citations, from one to thousands (fig. S2A).

2) The number of citations (*2*) collected by a paper strongly depends on the paper's age; hence, citation-based comparisons favor older papers and established investigators. It also lacks predictive power: A group of papers that within a 5-year span collect the same number of citations are found to have widely different long-term impacts (fig. S2B).

3) Paradigm-changing discoveries have notoriously limited early impact (*3*), precisely because the more a discovery deviates from the current paradigm, the longer it takes to be appreciated by the community (*16*). Indeed, although for most papers their early- and long-term citations correlate, this correlation breaks down for discoveries with the most long-term citations (Fig. 1B). Hence, publications with exceptional long-term impact appear to be the hardest to recognize on the basis of their early citation patterns.

4) Comparison of different papers is confounded by incompatible publication, citation, and/or acknowledgment traditions of different disciplines and journals.

Long-term cumulative measures like the Hirsch index have predictable components that can be extracted via data mining (*4*, *17*). Yet, given the myriad of factors involved in the recognition of a new discovery, from the work's intrinsic value to timing, chance, and the publishing venue, finding regularities in the citation history of individual papers, the minimal carriers of a scientific discovery, remains an elusive task.

In the past, much attention has focused on citation distributions, with debates on whether they follow a power law (*2*, *18*, *19*) or a log-normal form (*3*, *7*, *15*). Also, universality across disciplines allowed the rescaling of the distributions

[1]Center for Complex Network Research, Department of Physics, Department of Biology, and Department of Computer Science, Northeastern University, Boston, MA 02115, USA. [2]IBM Thomas J. Watson Research Center, Yorktown Heights, NY 10598, USA. [3]Department of Physics, University of Miami, Coral Gables, FL 33124, USA. [4]Center for Cancer Systems Biology, Dana Farber Cancer Institute, Boston, MA 02115, USA. [5]Department of Medicine, Brigham and Women's Hospital, Harvard Medical School, Boston, MA 02115, USA. [6]Center for Network Science, Central European University, Budapest, Hungary.

*These authors contributed equally to the work.
†Corresponding author. E-mail: alb@neu.edu